Simulating the emptying of a water bottle with a multi-scale two-fluid approach

Samuel Mer, Olivier Praud, Jacques Magnaudet, Véronique Roig

Proceedings of the ASME 2018 5th Joint US-European Fluids Engineering Summer Conference
FEDSM2018
July 15-20, 2018, Montreal, Quebec, Canada

FEDSM2018-83196

SIMULATING THE EMPTYING OF A WATER BOTTLE WITH A MULTI-SCALE TWO-FLUID APPROACH

Samuel Mer
Institut de Mécanique des Fluides de Toulouse
IMFT
Université de Toulouse - CNRS
Toulouse - France
Email: samuel.mer@imft.fr

Olivier Praud
Institut de Mécanique des Fluides de Toulouse
IMFT
Université de Toulouse - CNRS
Toulouse - France
Email: olivier.praud@imft.fr

Jacques Magnaudet
Institut de Mécanique des Fluides de Toulouse
IMFT
Université de Toulouse - CNRS
Toulouse - France
Email: jacques.magnaudet@imft.fr

Véronique Roig
Institut de Mécanique des Fluides de Toulouse
IMFT
Université de Toulouse - CNRS
Toulouse - France
Email: veronique.roig@imft.fr

ABSTRACT

Multiple industrial processes involve gas-liquid flows characterized by a wide range of spatial and temporal scales. Simulating such flows remains a major challenge nowadays, as the computational cost associated with Direct Numerical Simulation still makes it unaffordable. For such configurations, an interesting alternative to DNS is the use of multi-scale approaches. In the latter, large enough bubbles are fully resolved and may deform over time, while smaller bubbles are modeled as a dispersed phase using subgrid scale models. The interfacial momentum transfer terms are then tailored to the local flow configuration. The closure models still involved in these approaches and the influence of the cut-off length separating the resolved and modeled bubbles definitely need to be validated against detailed experiments. In order to assess the validity of these models, we present a one-to-one comparison between experiments performed in a simple configuration, namely the emptying of a water bottle, and numerical simulations using the aforementioned approach. The results are found to reliably reproduce the genesis of the oscillation mechanism, which is governed by the bubble formation at the bottle neck. The multi-scale model also qualitatively reproduces the fragmentation process of large bubbles during their rise in the water column. However local experimental data are required to assess more quantitatively these results.

NOMENCLATURE

ρ_k Density of phase k.
α_k Volume fraction of phase k.
μ_k Dynamic viscosity of phase k.
$\mathbf{u}_k$ Velocity vector of phase k.
σ Surface tension.
$\Gamma_{p\to k}$ Interfacial mass transfer rate from phase p to k.
$\mathbf{I}_{p\to k}$ Interfacial momentum transfer rate from phase p to k.
p Pressure.
T Temperature.
R_{air} Ideal gas constant.

INTRODUCTION

Multiphase gas-liquid flows are encountered in a broad spectrum of geophysical, environmental and industrial applications. As an example in the latter category, chemical industry makes an extensive use of bubble columns and plumes to enhance aeration or mixing. Nuclear design also requires reliable predictions of evaporation and water-steam flows in order to optimize plant design and safety. Such applications generally involve complex dispersed flows in which a wide range of bubble sizes coexist, such as in air entrainment configurations below an air-water interface. They may also involve transient flows that do not fall within a well-defined two-phase regime, as in cases where the flow configuration stands in between dispersed and churn flow regimes, or when free-surface oscillations at the top of a tank are coupled with the injection of a bubbly jet at its bottom.

In the recent decades, a significant effort has been carried out in the research community ([1–5]), especially in the context of the NEPTUNE_CFD solver project ([6–10]), to adapt the two-fluid model initially formalized by Ishii [11], to handle more complex flow configurations involving a wide range of bubble sizes and shapes or flow regime transitions. In such configurations, the largest bubbles or the large gas-liquid interfaces are allowed to deform freely and are captured numerically while the smaller ones are modeled within the framework of a dispersed bubbly flow formulation.

In this paper we present one of these multi-scale approaches, namely the Generalized Large Interface Model (GLIM) grounded on the Large Interface Model proposed by Coste [6] and updated by Merigoux et al [9]. We first describe the model in some detail before assessing its performances through a one-to-one comparison with experimental data corresponding to a relevant and original test case. The latter consists in the 'glug-glug' emptying process of an ideal water bottle. This flow configuration is of particular interest here since it involves complex physical phenomena with a broad range of spatio-temporal scales and leads to several successive flow transitions. Bubbles are created periodically at the bottle neck, typically with a diameter close to that of the neck. Then they detach from it and rise within the bottle until the free surface. While ascending, these large bubbles undergo break-up, and a swarm of smaller bubbles is generated, a fraction of which may coalesce again or participate in the reconfiguration of the largest bubbles; the larger the bottle neck the more intense these reconfigurations.

NUMERICAL MODEL

All the simulations discussed below were carried out with the NEPTUNE_CFD code [12–14] jointly developed by EdF, CEA, IRSN and AREVA in France. This flow solver describes multiphase flows in an Eulerian framework thanks to an extension to n fields of the two-fluid model established by Ishii [11]. This technique is particularly well suited for dispersed flows with a unique particle/drop/bubble size. In this context, two fields (also referred to as phases) are defined, namely a continuous liquid phase and a dispersed gas phase. In the general framework of a n-field approach, mass, momentum and energy balance equations are solved for each field, with the assumption of a common pressure shared by all of them. Our simulations assume an isothermal flow. Hence, no energy balance is considered. Since the GLIM approach is mostly an extension of the two-fluid model, we briefly go through the original model before presenting the multi-scale treatment.

Original two-fluid model

In an isothermal configuration, two balance equations are solved in each phase. The mass balance in phase k reads

$$\frac{\partial}{\partial t}(\alpha_k \rho_k) + \nabla \cdot (\alpha_k \rho_k \mathbf{u}_k) = \sum_{p \neq k} \Gamma_{p \to k}\,, \tag{1}$$

where α_k denotes the local volume fraction of phase k, ρ_k its density, $\mathbf{u}_k$ its mass-averaged velocity and $\Gamma_{p\to k}$ stands for the interfacial mass transfer rate between phases p and k. No phase change is considered in the present simulations, implying $\Gamma_{p\to k} = 0$.

The momentum balance is also solved in each phase in the form

$$\begin{aligned} \tfrac{\partial}{\partial t}(\alpha_k \rho_k \mathbf{u}_k) + \nabla \cdot (\alpha_k \rho_k \mathbf{u}_k \otimes \mathbf{u}_k) &= -\alpha_k \nabla P + \alpha_k \rho_k \mathbf{g} \\ + \nabla \cdot \left(\alpha_k \mu_k (\nabla \mathbf{u}_k + {}^{\mathrm{T}} \nabla \mathbf{u}_k)\right) &+ \sum_{p \neq k} \mathbf{I}_{p \to k}\,, \end{aligned} \tag{2}$$

where μ_k denotes the viscosity of phase k and $\mathbf{I}_{p\to k}$ stands for the interfacial momentum transfer rate between phases p and k.

The interfacial momentum transfer term can be decomposed into two contributions in the form

$$\mathbf{I}_{p\to k} = \mathbf{I}^{hydro}_{p\to k} + \Gamma_{p\to k}(\mathbf{u}_p - \mathbf{u}_k)^{int}\,,$$

where the subscript int denotes the quantity evaluated at the interface between phases p and k. As no phase change is considered here, the second contribution is zero and only $\mathbf{I}^{hydro}_{p\to k}$ needs to be modeled to close the full set of equations. When considering bubbly flows involving mono-dispersed bubbles, NEPTUNE_CFD uses closures for $\mathbf{I}^{hydro}_{p\to k}$ that were already validated on several industrial configurations [10] [14]. In such situations, the interfacial momentum transfer $\mathbf{I}^{hydro}_{cl\to dg}$ (subscripts cl and dg refer to the carrying liquid and the dispersed gas phase, respectively) is decomposed into three contributions, namely a drag force $\mathbf{F}^{drag}$, a lift force $\mathbf{F}^{lift}$, and an added-mass force $\mathbf{F}^{am}$.

The reader is referred to [15] for the complete expression of each

of these terms. However, these closures are mostly based on specific empirical validations, which greatly limits their universality. When dealing with multi-scale flows, the mono-disperse assumption is not valid any longer and new treatments are required to deal with bubbles much larger than the grid resolution.

Generalized Large interface Model

The GLIM is an extension of the LIM model proposed by Coste [6] to simulate separated (stratified) two-phase flows where a liquid layer is sheared by a high-velocity gas flow. The main ingredients of the model are presented below. In what follows, subscripts cl and cg refer to the continuous liquid and gas phases, respectively.

Large Interface Detection A large interface (LI) is represented by a three-cell stencil (LI3C method [6]). In this stencil, the central cell contains the interface, with a mixture of the two phases (*i.e.* $\alpha_{cl}\alpha_{cg} \neq 0$), and one cell on each side of the interface contains only one phase (*i.e.* $\alpha_{cl} = 0$ or $\alpha_{cg} = 0$). The former cell is detected thanks to the local value of the liquid volume fraction gradient, $\nabla\alpha_{cl}$. More details on the detection algorithm can be found in [6]. Here it is enough to indicate that the detection consists essentially in comparing each component of the gradient to a pre-defined threshold value. Then the liquid and gas cells are detected by moving away by one cell in the direction normal to the interface. This gives access to liquid/gas velocities and liquid/gas cell distances to the interface which are necessary to express the momentum exchange terms.

Large Interface Interfacial Momentum Transfer Once large interfaces are detected, the interfacial momentum transfer term involved in Eq. 2 is set to a nonzero value only in cells containing such large interfaces. This interfacial momentum transfer essentially results from the friction between the two phases in the interface region. Hence $\mathbf{I}^{hydro}_{cl\to cg}$ is closed in the form

$$\mathbf{I}^{hydro}_{cl\to cg} = \rho_g u^{*2}_{cg} A_i \frac{(\mathbf{u}_{cl} - \mathbf{u}_{cg})}{||\mathbf{u}_{cl} - \mathbf{u}_{cg}||}, \tag{3}$$

where A_i denotes the interfacial area rate and u^*_{cg} is the gas friction velocity which depends on the interface deformation. The interfacial area rate is defined as $A_i = S_i/V$, S_i being the interface area contained within the cell volume V. Clearly this model assumes that a nonzero slip exists between the two phases across a large interface. The interface deformation regime, hence the friction velocity u^*_{cg}, is determined based on the Brocchini-Peregrine diagram [16, 17] which gathers various situations, some of which involve strong turbulence interacting with gas-liquid interfaces. The frictional force defined in Eq. 3 proved to be crucial in the modeling of separated two-phase flows with a liquid layer sheared by a gas flow.

Actually, an additional term is added to $\mathbf{I}^{hydro}_{cl\to cg}$ for numerical purpose. The role of this term is to enforce the equality of the normal component of the gas and liquid velocities at a large interface. This is achieved by introducing a penalization force in the direction normal to the interface in the form

$$\mathbf{F}^{LI}_{cl\to cg} = \alpha_{cl}\alpha_{cg}(\alpha_{cg}\rho_g + \alpha_{cl}\rho_l)\frac{C_\tau}{\Delta t}\left[(\mathbf{u}_{cl} - \mathbf{u}_{cg})\cdot\mathbf{n}\right]\mathbf{n}, \tag{4}$$

where C_τ is an empirical coefficient of order unity, Δt the numerical time step, and $\mathbf{n} = \nabla\alpha_{cl}/||\nabla\alpha_{cl}||$ denotes the unit normal to the LI. As shown by Eq. 4, any difference between the normal components of $\mathbf{u}_{cl}$ and $\mathbf{u}_{cg}$ on a LI (which is the only flow region where the product $\alpha_{cl}\alpha_{cg}$ is nonzero) results in a large normal force $\mathbf{F}^{LI}_{cl\to cg}$ if Δt is small. Hence, selecting a large value of $C_\tau/\Delta t$ guarantees that the difference between the two normal velocity components is negligibly small at the interface.

Interfacial Momentum Transfer For The Dispersed Gas Phase As the simulation proceeds, depending on the flow configuration, many cells may not contain any large interface although the local gas volume fraction is different from zero. Such a configuration implies that dispersed bubbles are locally present, and the proper interfacial momentum exchange term has to be modified to deal with this specific flow structure. This is typically the case when simulating the 'glug-glug' generated by the emptying of a bottle.

To deal with this configuration, the interfacial momentum transfer term is tailored to the local flow structure in the following manner. First, the large interface detection algorithm is applied to detect large interfaces throughout the domain. If a LI is detected, the LI momentum transfer term, defined in Eqs. 3 and 4, is prescribed at the corresponding location. Then, in cells that do not contain any large interface but where the local gas volume fraction is nonzero, the dispersed interfacial momentum transfer terms $\mathbf{F}^{drag}_{cl\to dg}$, $\mathbf{F}^{lift}_{cl\to dg}$ and $\mathbf{F}^{am}_{cl\to dg}$ are prescribed. To avoid any overlap between the two models at a given location, the entire momentum exchange term for the dispersed phase, $\mathbf{I}^{hydro}_{cl\to dg}$, is weighted against an empirical numerical parameter, ω. This parameter was calibrated based on the feedback gained during the validation of the overall model [9]. It reads

$$\omega = \beta\,(1 - Min(6 f_{cor}, 1)) \quad \text{with} \quad f_{cor} = A_i^{-1}||\nabla\alpha_l||. \tag{5}$$

In Eq. 5, β is a pre-factor that smoothly varies from 0 to 1 according to the local value of the liquid volume fraction α_l. More specifically, β is set to 0 if $\alpha_l < 0.5$, which is considered to correspond to locations involving large interfaces. Conversely, $\beta = 1$

if $\alpha_l > 0.7$, *i.e.* at locations where the flow structure is considered to be dominated by the presence of dispersed bubbles. Last, β follows the linear variation $\beta = (\alpha_l - 0.5)/0.2$ if $0.5 \leq \alpha_l \leq 0.7$.

The factor f_{cor} takes into account the presence of large interfaces: such interfaces result in large values of f_{cor}, hence small (if not zero) ω, reducing the overall momentum transfer term to that defined in Eq. 3 . Figure 1 provides a sketch of the combined effect of β and f_{cor} on the value of ω in a typical cell.

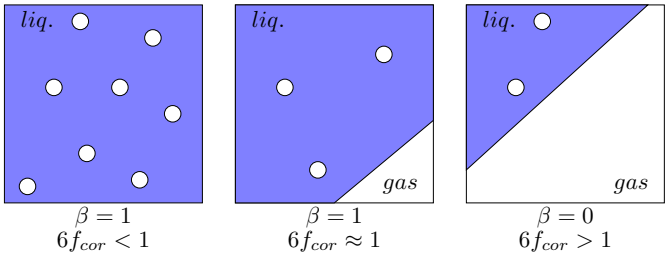

FIGURE 1: THE ROLE OF f_{cor} AND β IN THE WEIGHTING PROCEDURE OF THE INTERFACE MODEL WITHIN A CELL.

DESCRIPTION OF THE TEST CASE

In order to assess the validity of the above model, the experimental configuration detailed in [15] is reproduced numerically. The bottle is schematized as a cylinder with diameter $D = 114\,\text{mm}$ and height $L = 800\,\text{mm}$, closed at the top by a blank flange and at the bottom by a perforated plate mimicking the bottle neck. In the simulations, the neck diameter is set to $d = 35\,\text{mm}$ and a fixed initial normalized water height, $H/L = 0.75$ is imposed. The simulations are run over 5 s, with a fixed time step of 0.05 ms.

The computational domain is sketched in Fig. 2. In order to avoid disturbances resulting from the outlet boundary condition, an air buffer region is added between the bottle neck and the outlet. All other boundaries are treated as rigid walls corresponding to a no-slip condition. The simulation makes use of a 3D grid dividing the domain into ≈ 2.1 millions nonuniform hexahedral cells. With this grid, the dispersed bubble diameter is set to $1\,mm$. It yields a bubble volume about 40% of the averaged cell volume, which is consistent with the dispersed phase assumptions and allows us to properly resolve a significant part of the gas content. Initially, the liquid and gas phases are at rest. Within the two regions filled with air (see Fig. 2), the pressure is initially set to the same constant value corresponding to the atmospheric pressure. In contrast, a hydrostatic pressure distribution is considered initially within the water column.

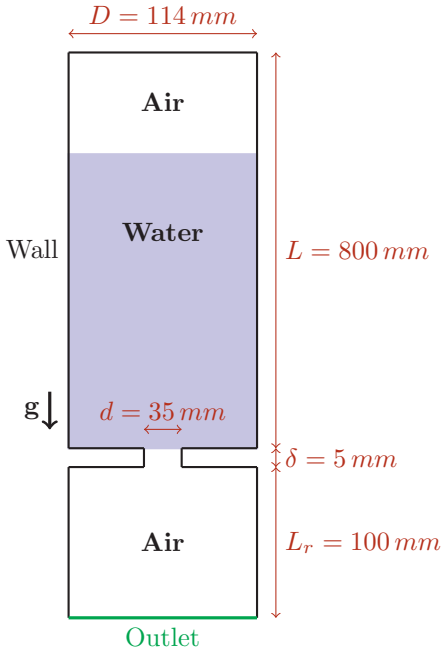

FIGURE 2: 2D SKETCH OF THE COMPUTATIONAL DOMAIN.

Water properties are extracted from the CATHARE module embedded in the NEPTUNE_CFD code. Considering a uniform and constant temperature $T = 293.15\,\text{K}$, one has $\rho_l = 997.24\,\text{kg.m}^{-3}$ and $\mu_l = 1 \times 10^{-3}\,\text{Pa.s}$. Based on the companion study [15], the air phase is considered compressible and assumed to behave as an an isothermal ideal gas. The air density, ρ_a, and its partial derivative with respect to the pressure, p, obey respectively $\rho_a = p(R_{air}T)^{-1}$ and $(\partial\rho_a/\partial p)_T = (R_{air}T)^{-1}$, with $R_{air} = 287.06\ \text{J.kg}^{-1}\text{.K}^{-1}$. The air viscosity and the water/air surface tension are respectively set to $\mu_a = 1.8 \times 10^{-5}\,\text{Pa.s}$ and $\sigma = 7.28 \times 10^{-2}\text{N.m}$.

RESULTS AND DISCUSSION

Analysis Of The Pressure Signal At The Bottle Top

Figure 3 depicts the experimental and numerical pressure signals at the bottle top (the atmospheric pressure was systematically removed from the signal to highlight pressure variations within the bottle). It appears that the amplitude of the numerical oscillations is significantly underestimated compared to the experimental findings during the first second of the emptying process. After this initial transient, the numerical amplitudes are in much better agreement with the experimental evolution. Two markedly different time scales are involved in the pressure signal. On the one hand, a gentle linear pressure increase is observed over a long time scale. This feature is due to the gradual

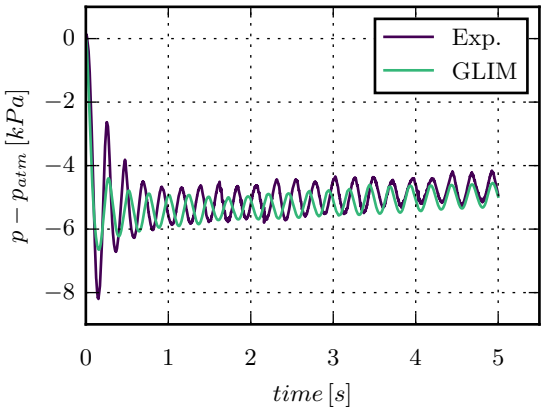

FIGURE 3: NUMERICAL AND EXPERIMENTAL PRESSURE EVOLUTIONS AT THE BOTTLE TOP.

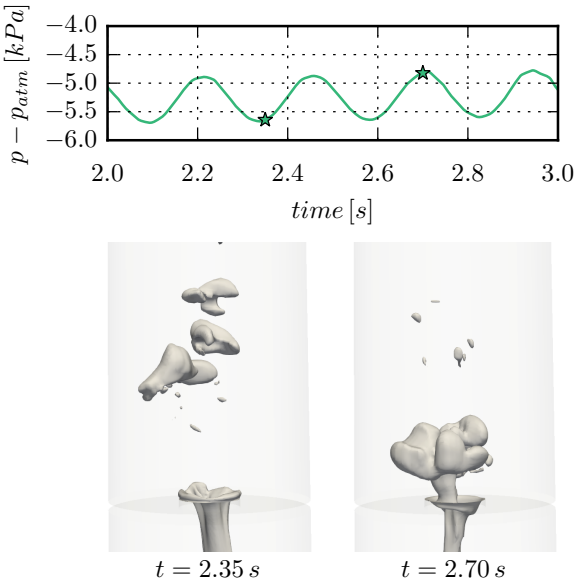

FIGURE 4: VISUALIZATION OF THE SYNCHRONIZATION BETWEEN BUBBLE FORMATION AND PRESSURE OSCILLATIONS.

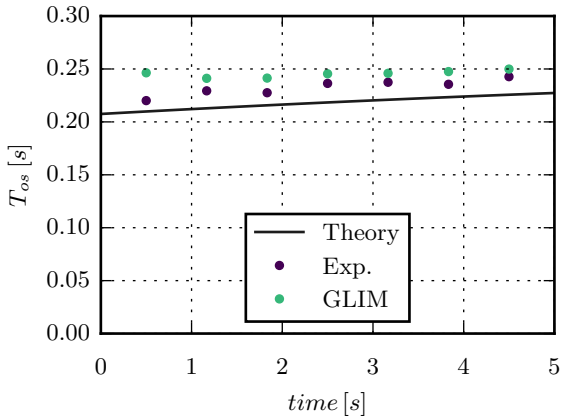

FIGURE 5: EVOLUTION OF THE PRESSURE OSCILLATION PERIOD. THE NUMERICAL SIGNAL IS COMPARED WITH THE EXPERIMENTAL ONE AND WITH THE THEORETICAL MODEL OF [18].

reduction of the liquid height within the bottle [15]. On the other hand, high frequency oscillations are superimposed to this linear increase. These oscillations are mainly due to the periodic bubble generation and liquid ejection at the neck, as revealed in Fig. 4. In this figure, snapshots of bubble formation and liquid ejection at the bottle neck are displayed, together with the pressure oscillations at the top of the bottle. Bubble formation is seen to correspond to a pressure rise, whereas liquid ejection takes the form of a jet and corresponds to a pressure minimum. Indeed, bubble formation at the neck induces a rise of the free surface, thus a compression of the air buffer at the bottle top. In contrast, liquid ejection decreases the volume of liquid within the bottle, inducing an expansion of the air buffer which in turn reduces the pressure.

Coming back to pressure oscillations displayed in Fig. 3, the numerical period is observed to be slightly longer than the experimental one, as shown in more detail in Fig. 5. The period reported in this figure was obtained after a sliding Fourier transform was applied to the pressure signal. This figure confirms that the numerical prediction overestimates the actual period. The difference reaches a maximum at the beginning of the emptying process and reduces over time, its relative value ending within a few percents.

Analysis of Bubble Swarms

In such multi-scale bubbly flow configurations, a natural concern is the structure of bubble swarms. A first step toward the analysis of these swarms is provided in Fig. 6, where the experimental structure, revealed though a shadowgraph technique, is compared with the numerical prediction at the instant of time $t = 4.2\,\mathrm{s}$. Large bubbles are identified by the iso-contour $\alpha_{cl} = 0.5$, whereas dispersed bubbles are represented with a depth-integrated color scale. It must be pointed out that in the experimental case, the initial water height is $H/L = 1$, whereas it is only 0.75 in the simulation. Hence the two cases reported in Fig. 6 have different flow histories. In particular, the population of small bubbles in the experiment may well be denser than if the initial relative height were 0.75.

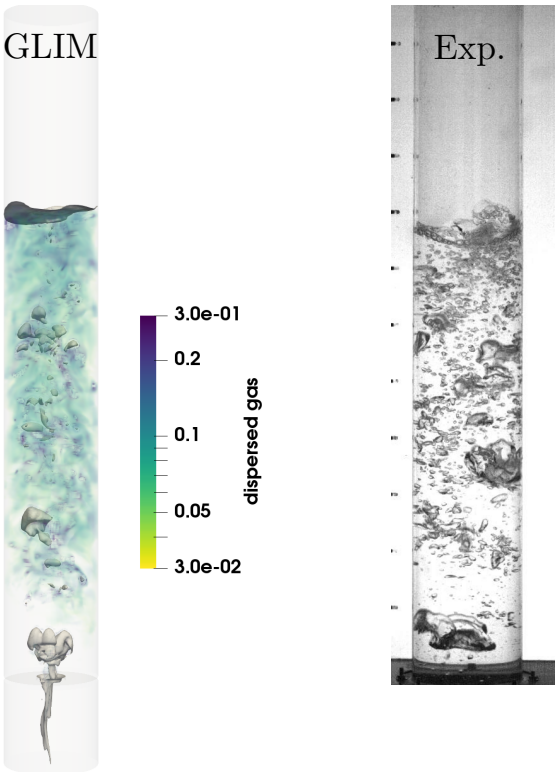

FIGURE 6: VISUALIZATION OF BUBBLE SWARMS IN THE WATER COLUMN (LEFT: SIMULATION, RIGHT: EXPERIMENT). LARGE INTERFACES ARE IDENTIFIED BY THE ISO-CONTOUR $\alpha_{cl} = 0.5$. THE COLOR SCALE REPRESENTS THE DISPERSED GAS PHASE.

Despite this difference, a fairly good resemblance is noticed between the two images, with the formation of large bubbles at the neck, which then break-up during their rise in the water column and generate smaller and smaller bubbles. With the selected grid resolution, these small bubbles are not resolved and belong to the dispersed gas phase; their presence may be appreciated through the color scale in Fig. 6. Although only qualitative, the resemblance between the two snapshots suggests that the model is capable of handling transitional regimes involving successive fragmentation events. However the experimental visualization is too global to allow any quantitative comparison. To obtain a slightly more quantitative insight into the generation of the dispersed bubble phase, the evolution of the cross-sectional average gas fraction at two different heights is plotted in Fig. 7. The average is performed within a 1 cm thick cylindrical control volume with diameter D centered at height h_{cv}. In the left panel, corresponding to a cross section located $h_{cv} = 10\,\text{cm}$ above the bottle neck, the gas fraction exhibits a series of sharp peaks. Each of them corresponds to the crossing of the control volume by a large gas bubble. The peak magnitude depends on several parameters, such as the bubble size, shape and orientation. Hence the volume fraction signal is not sufficient to extract a quantitative information on the bubble characteristics. The right panel in Fig. 7 displays the same quantity within a control volume located significantly higher in the bottle, *i.e.* $h_{cv} = 30\,\text{cm}$ above the neck. The time evolution is split into two different windows to provide a clearer view of the events that take place in each of them. The early evolution reveals few, albeit sharp, peaks. The average gas fraction rises on average and roughly stabilizes itself on a 'plateau' value $\approx 7\%$. This rise corresponds to the generation of a swarm of small bubbles in the water column, associated with the fragmentation of a large bubble. On a longer term, some large bubbles still rise in the water column. Their signature corresponds to the peaks that still make the average volume fraction deviate from time to time from its plateau value. These features suggest that the model allows successive bubble fragmentations but at the same time maintains the presence of some large bubbles until the free surface. We are not aware of any detailed experimental data that would allow us to validate quantitatively the numerical evolution of the gas fraction displayed in Fig. 7. Hence, further experimental investigations are necessary to quantitatively assess the validity of present computational results.

CONCLUSIONS

We reported two-phase flow multi-scale simulations based on the Eulerian code NEPTUNE_CFD in the non-trivial configuration corresponding to the emptying of a bottle. This test case involves a broad range of bubble sizes, from large gas pockets formed at the neck to tiny bubbles resulting from fragmentation. All these bubbles strongly interact during the emptying process.These features make this test case relevant to evaluate recent models intended to jointly resolve large interfaces and model the influence of small bubbles.

Present simulations reveal the existence of large pressure oscillations within the bottle, the frequency of which is locked on the detachment of large bubbles at the bottle neck. The numerical model was found to properly reproduce this frequency, except during the initial transient stage. A qualitative comparison with experimental visualizations suggests that the numerical approach based on the Large Interface Model allows bubbles to properly break-up and reconfigure through fragmentation, in qualitative overall agreement with experimental observations.

Measurements of the gas volume fraction, possibly supplemented with an evaluation of the bubble size distribution throughout the bottle, are now necessary to quantitatively assess the predictions of this model.

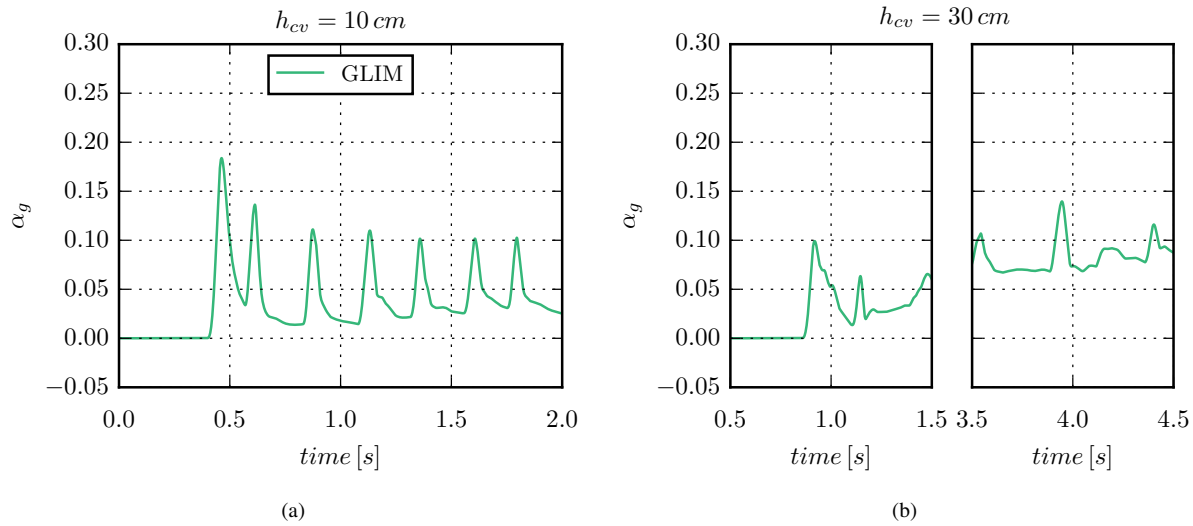

(a) (b)

FIGURE 7: TIME EVOLUTION OF THE CROSS-SECTIONAL AVERAGE GAS FRACTION AT DIFFERENT HEIGHTS. THE MEASUREMENT VOLUME IS 1 cm THICK, WITH ITS CENTER SET AT HEIGHT h_{cv} ABOVE THE NECK.

ACKNOWLEDGMENT

This work was granted access to the HPC resources of the CALMIP supercomputing center under the allocation P17034.

REFERENCES

[1] Henriques, A., 2006. "Prise en compte des grandes interfaces dans un code moyenné eulérien à deux champs de vitesse". PhD thesis, Inst. Nat. Polytech. Grenoble, France.

[2] Krepper, E., Lucas, D., Frank, T., Prasser, H. M., and Zwart, P. J., 2008. "The inhomogeneous MUSIG model for the simulation of polydispersed flows". Nuclear Engineering and Design, **238**, pp. 1690–1702.

[3] Strubelj, L., 2009. "Numerical simulations of stratified two-phase flows with two-fluid model and interface sharpening". PhD thesis, Ljublana Univ., Slovenia.

[4] Hansch, S., Lucas, D., Krepper, E., and Hohne, T., 2012. "A multi-field two-fluid concept for transitions between different scales of interfacial structures". International Journal of Multiphase Flow, **47**, pp. 171–182.

[5] Montoya, G., Baglietto, E., and Lucas, D., 2015. "Implementation and validation of a surface tension model for the multi-scale approach gentop". In International Topical Meeting on Nuclear Reactor Thermal Hydraulics 2015, NURETH 2015, Vol. 5, pp. 4219–4232.

[6] Coste, P., 2013. "A large interface model for two-phase CFD". Nuclear Engineering and Design, **255**, pp. 38–50.

[7] Denèfle, R., Mimouni, S., Caltagirone, J.-P., and Vincent, S., 2015. "Multifield hybrid approach for two-phase flow modeling - Part 1: Adiabatic flows". Computers & Fluids, **113**, pp. 106–111.

[8] Fleau, S., Mimouni, S., Mérigoux, N., and Vincent, S., 2015. "Simulations of two-phase flows with a multifield approach". In Proceedings of CHT-15. 6th International Symposium on Advances in Computational Heat Transfer, May 25-29, 2015, Rutgers Univ., New Brunswick, NJ, USA, pp. 78–96.

[9] Merigoux, N., Lavieville, J., Mimouni, S., Guingo, M., and Baudry, C., 2016. "A Generalized Large Interface to dispersed bubbly flow approach to model two-phase flows in nuclear power plant". In CFD4NRS-6, September 13-15, 2016, Cambridge, MA - USA, pp. 1–20.

[10] Fleau, S., Mimouni, S., Merigoux, N., and Vincent, S., 2016. "Validation of a multifield approach for the simulations of two-phase flows". Computational Thermal Sciences, **7**, pp. 441–457.

[11] Ishii, M., 1975. Thermo-Fluid Theory of Two-Phase Flow. Eyrolles, Paris.

[12] Mimouni, S., Lamy, J.-S., Lavieville, J., Guieu, S., and Martin, M., 2010. "Modelling of sprays in containment applications with A CMFD code". Nuclear Engineering and Design, **240**(9), sep, pp. 2260–2270.

[13] Mimouni, S., Foissac, A., and Lavieville, J., 2011. "CFD modelling of wall steam condensation by a two-phase flow approach". Nuclear Engineering and Design, **241**(11), pp. 4445–4455.

[14] Mimouni, S., Laviéville, J., Seiler, N., and Ruyer, P., 2011. "Combined evaluation of second order turbulence model and polydispersion model for two-phase boiling flow and application to fuel assembly analysis". Nuclear Engineering and Design, **241**, pp. 4523–4536.

[15] Mer, S., Praud, O., Merigoux, N., Neau, H., Magnaudet, J., and Roig, V., 2018. "The emptying of a bottle as a test case for assessing interfacial momentum exchange models for Euler-Euler simulations of multi-scale gas-liquid flows". International Journal of Multiphase Flow, (submitted).

[16] Brocchini, M., and Peregrine, D., 2001. "The dynamics of strong turbulence at free surfaces. Part 1. Description". Journal of Fluid Mechanics, **449**, pp. 225–254.

[17] Brocchini, M., and Peregrine, D., 2001. "The dynamics of strong turbulence at free surfaces. Part 2. Free-surface boundary conditions". Journal of Fluid Mechanics, **449**, pp. 255–290.

[18] Clanet, C., and Searby, G., 2004. "On the glug-glug of ideal bottles". Journal of Fluid Mechanics, **510**, pp. 145–168.